



**HAL**  
open science

## Second harmonic imaging and scoring of collagen in fibrotic tissues.

Mathias Strupler, Ana-Maria Pena, Monica Hernest, Pierre-Louis Tharaux, Jean-Louis Martin, Emmanuel Beaurepaire, Marie-Claire Schanne-Klein

► **To cite this version:**

Mathias Strupler, Ana-Maria Pena, Monica Hernest, Pierre-Louis Tharaux, Jean-Louis Martin, et al.. Second harmonic imaging and scoring of collagen in fibrotic tissues.. Optics Express, 2007, 15 (7), pp.4054-4065. 10.1364/OE.15.004054 . hal-00824058

**HAL Id: hal-00824058**

**<https://polytechnique.hal.science/hal-00824058>**

Submitted on 13 Nov 2013

**HAL** is a multi-disciplinary open access archive for the deposit and dissemination of scientific research documents, whether they are published or not. The documents may come from teaching and research institutions in France or abroad, or from public or private research centers.

L'archive ouverte pluridisciplinaire **HAL**, est destinée au dépôt et à la diffusion de documents scientifiques de niveau recherche, publiés ou non, émanant des établissements d'enseignement et de recherche français ou étrangers, des laboratoires publics ou privés.

# Second harmonic imaging and scoring of collagen in fibrotic tissues

M. Strupler, A.-M. Pena, and M. Hernest

*Laboratoire d'Optique et Biosciences; Ecole Polytechnique; CNRS; INSERM U696, 91128 Palaiseau, France*

P.-L. Tharaux

*INSERM U689; Centre de Recherche Cardiovasculaire Inserm Lariboisière, 75010 Paris, France*

J.-L. Martin, E. Beaupaire, and M.-C. Schanne-Klein

*Laboratoire d'Optique et Biosciences; Ecole Polytechnique; CNRS; INSERM U696, 91128 Palaiseau, France*  
[marie-claire.schanne-klein@polytechnique.edu](mailto:marie-claire.schanne-klein@polytechnique.edu)

**Abstract:** We compare second harmonic generation (SHG) to histological and immunohistochemical techniques for the visualization and scoring of collagen in biological tissues. We show that SHG microscopy is highly specific for fibrillar collagens and that combined SHG and two-photon excited fluorescence (2PEF) imaging can provide simultaneous three-dimensional visualization of collagen synthesis and assembly sites in transgenic animal models expressing GFP constructs. Finally, we propose several scores for characterizing collagen accumulation based on SHG images and appropriate for different types of collagen distributions. We illustrate the sensitivity of these scores in a murine model of renal fibrosis using a morphological segmentation of the tissue based on endogenous 2PEF signals.

©2007 Optical Society of America

**OCIS codes:** (190.4160) Multiharmonic generation; (180.6900) Three-dimensional microscopy; (110.4280) Noise in imaging systems; (170.3880) Medical and biomedical imaging.

---

## References and links

1. P. J. Campagnola, A. C. Millard, M. Terasaki, P. E. Hoppe, C. J. Malone and W. A. Mohler, "Three-dimensional high-resolution Second-Harmonic Generation imaging of endogenous structural proteins in biological tissues," *Biophys. J.* **82**, 493-508 (2002).
2. A. Zoumi, A. Yeh and B. J. Tromberg, "Imaging cells and extracellular matrix in vivo by using second-harmonic generation and two-photon excited fluorescence," *Proc. Natl. Acad. Sci. USA* **99**, 11014-11019 (2002).
3. G. Cox, E. Kable, A. Jones, I. Fraser, K. Marconi and M. D. Gorrell, "3-dimensional imaging of collagen using second harmonic generation," *J. Struct. Biol.* **141**, 53-62 (2003).
4. E. Brown, T. Mckee, E. Ditomaso, A. Pluen, B. Seed, Y. Boucher and R. K. Jain, "Dynamic imaging of collagen and its modulation in tumors in vivo using second-harmonic generation," *Nat. Med.* **9**, 796-800 (2003).
5. P. Stoller, P. M. Celliers, K. M. Reiser and A. M. Rubenchik, "Quantitative second-harmonic generation microscopy in collagen," *Appl. Opt.* **42**, 5209-5219 (2003).
6. W. R. Zipfel, R. M. Williams, R. Christie, A. Y. Nikitin, B. T. Hyman and W. W. Webb, "Live tissue intrinsic emission microscopy using multiphoton-excited native fluorescence and second harmonic generation," *Proc. Natl. Acad. Sci. USA* **100**, 7075-7080 (2003).
7. K. König and I. Riemann, "High-resolution multiphoton tomography of human skin with subcellular spatial resolution and picosecond time resolution," *J. Biomed. Opt.* **8**, 432-439 (2003).
8. A.-M. Pena, M. Strupler, T. Boulesteix, G. Godeau and M.-C. Schanne-Klein, "Spectroscopic analysis of keratin endogenous signal for skin multiphoton microscopy," *Opt. Express* **13**, 6268-6274; erratum: **13**(17) 6667 (2005).
9. J. A. Palero, H. S. D. Bruijn, A. V. D. P.-V. D. Heuvel, H. J. C. M. Sterenborg and H. C. Gerritsen, "In vivo nonlinear spectral imaging in mouse skin," *Opt. Express* **14**, 4395-4402 (2006).

10. T. Boulesteix, A. M. Pena, N. Pagès, G. Godeau, M.-P. Sauviat, E. Beaufrepaire and M. C. Schanne-Klein, "Micrometer scale ex vivo multiphoton imaging of unstained arterial wall structure," *Cytometry* **69A**, 20-26 (2006).
11. A.-M. Pena, T. Boulesteix, T. Dartigalongue and M.-C. Schanne-Klein, "Chiroptical effects in the second harmonic signal of collagens I and IV," *J. Am. Chem. Soc.* **127**, 10314-10322 (2005).
12. S.-J. Lin, R.-Jr Wu, H.-Y. Tan, W. Lo, W.-C. Lin, T.-H. Young, C.-J. Hsu, J.-S. Chen, S.-H. Jee and C.-Y. Dong, "Evaluating cutaneous photoaging by use of multiphoton fluorescence and second-harmonic generation microscopy," *Opt. Lett.* **30**, 2275-2277 (2005).
13. M. J. Koehler, K. König, P. Elsner, R. Bückle and M. Kaatz, "In vivo assessment of human skin aging by multiphoton laser scanning tomography," *Opt. Lett.* **31**, 2879-2881 (2006).
14. A.-M. Pena, A. Fabre, D. Débarre, J. Marchal-Somme, B. Crestani, J.-L. Martin, E. Beaufrepaire and M.-C. Schanne-Klein, "Three-dimensional investigation and scoring of extracellular matrix remodeling during lung fibrosis using multiphoton microscopy," *Microsc. Res. Tech.* in press (2007).
15. A. Zoumi, X. Lu, G. S. Kassab and B. J. Tromberg, "Imaging coronary artery microstructure using second-harmonic and two-photon fluorescence microscopy," *Biophys. J.* **87**, 2778-2786 (2004).
16. K. Schenke-Layland, I. Riemann, U. A. Stock and K. König, "Imaging of cardiovascular structures using near-infrared femtosecond multiphoton laser scanning microscopy," *J. Biomed. Opt.* **10**, 024017 (2005).
17. N. Buyukbabani and D. Droz, "Distribution of the extracellular matrix components in human glomerular lesions," *J. Pathol.* **172**, 199-207 (1994).
18. M. S. Razaque, M. Cheng, Y. Horita, M. Nishihara, T. Harada and T. Taguchi, "Immunohistochemical analysis of type III and IV collagens in tubulointerstitial damage in human benign nephrosclerosis," *J. Int. Med. Res.* **23**, 480-486 (1995).
19. L. C. U. Junqueira, G. Bignolas and R. R. Brentani, "Picrosirius staining plus polarization microscopy, a specific method for collagen detection in tissue sections," *Histochem. J.* **11**, 447-155 (1979).
20. P. Whittaker, R. A. Kloner, D. R. Boughner and J. G. Pickering, "Quantitative assessment of myocardial collagen with picrosirius red staining and circularly polarized light," *Basic Res. Cardiol.* **89**, 397-410 (1994).
21. M. Oheim, E. Beaufrepaire, E. Chaigneau, J. Mertz and S. Chrapak, "Two-photon microscopy in brain tissue: parameters influencing the imaging depth," *J. Neurosci. Methods* **111**, 29-37 (2001).
22. D. Débarre, W. Suppato, A. M. Pena, A. Fabre, T. Tordjmann, L. Combettes, M. C. Schanne-Klein and E. Beaufrepaire, "Imaging lipid bodies in cells and tissues using third-harmonic generation microscopy," *Nat. Methods* **3**, 47 - 53 (2006).
23. K. L. Kusser and T. D. Randall, "Simultaneous detection of EGFP and cell surface markers by fluorescence Microscopy in Lymphoid Tissues," *J. Histochem. Cytochem.* **51**, 5-14 (2003).
24. W. Wang, J. B. Wyckoff, V. C. Frohlich, Y. Oleynikov, S. Hüttelmaier, J. Zavadil, L. Cermak, E. P. Bottinger, R. H. Singer, J. G. White, J. E. Segall and J. S. Condeelis, "Single cell behavior in metastatic primary mammary tumors correlated with gene expressions patterns revealed by molecular profiling," *Cancer Res.* **62**, 6278-6288 (2002).
25. W. Lo, S.-W. Teng, H.-Y. Tan, K. H. Kim, H.-C. Chen, H.-S. Lee, Y.-F. Chen, P. T. C. So and C.-Y. Dong, "Intact corneal stroma visualization of GFP mouse revealed by multiphoton imaging," *Microsc. Res. Tech.* **69**, 973-975 (2006).
26. Y. Yata, A. Scanga, A. Gillan, L. Yang, S. Reif, M. Breindl, D. A. Brenner and R. A. Rippe, "DNase I-hypersensitive sites enhance  $\alpha 1(I)$  collagen gene expression in Hepatic Stellate Cells," *Hepatology* **37**, 267-276 (2003).
27. J. Mertz and L. Moreaux, "Second-harmonic generation by focused excitation in inhomogeneously distributed scatterers," *Opt. Commun.* **196**, 325-330 (2001).
28. A. K. Dunn, V. P. Wallace, M. Coleno, M. W. Berns and B. J. Tromberg, "Influence of optical properties on two-photon fluorescence imaging in turbid samples," *Appl. Opt.* **39**, 1194-1201 (2000).
29. B. M. Kim, J. Eichler, K. M. Reiser, A. M. Rubenchik and L. B. Da Silva, "Collagen structure and nonlinear susceptibility: effects of heat, glycation, and enzymatic cleavage on second harmonic signal intensity," *Lasers Surg. Med.* **27**, 329-335 (2000).
30. R. M. Williams, W. R. Zipfel and W. W. Webb, "Interpreting second-harmonic generation images of collagen fibrils," *Biophys. J.* **88**, 1377-1386 (2005).
31. M. Han, G. Giese and J. F. Bille, "Second harmonic generation imaging of collagen fibrils in cornea and sclera," *Opt. Express* **13**, 5791-5797 (2005).
32. D. J. S. Hulmes, "Building collagen molecules, fibrils, and suprafibrillar structures," *J. Struct. Biol.* **137**, 2-10 (2002).
33. A. Fogo, J. A. Breyer, M. C. Smith, W. H. Cleveland, L. Agodoa, K. A. Kirk and R. Glassock, "Accuracy of the diagnosis of hypertensive nephrosclerosis in African Americans: a report from the African American Study of Kidney Disease (AASK) Trial. AASK pilot study investigators," *Kidney Int.* **51** (1997).
34. K. A. Nath, "Tubulointerstitial changes as a major determinant in the progression of renal damage," *Am. J. Kidney Dis.* **20**, 1-17 (1992).

## 1. Introduction

Collagen is routinely visualized using transmitted light microscopy of histological sections stained with Masson's trichrome or picrosirius red or, in some cases, using fluorescence microscopy of immunolabeled sections. More recently, second harmonic generation (SHG) microscopy has been used to visualize unstained collagenous tissues, in combination with two-photon excited fluorescence (2PEF) from elastin, keratin, and endogenous cellular chromophores [1-10]. Comparison with picrosirius red staining and anti-collagen I immunolabeling showed that endogenous SHG signals arise from fibrillar collagen, whereas no SHG signals were observed from collagen IV in the basal laminae [2-4, 11]. However, SHG microscopy has not yet been fully characterized in terms of its specificity, versatility and applicability for accurate measurements in collagenous tissues. In particular, few studies extracted quantitative information from SHG images for biomedical applications: a SHG-to-endogenous fluorescence ratiometric index has been proposed in the dermis [12, 13], and our group recently proposed scores using SHG microscopy for assessing the extent of pulmonary fibrosis in a murine model, which successfully sorted out fibrotic and control animals [14].

In this study, we propose a refined strategy for acquiring and processing SHG images and we present sensitive measurements of the accumulation of fibrillar collagen in kidney tissue. We first thoroughly compare SHG microscopy to conventional optical techniques for visualizing fibrillar collagen, in particular to polarized-light microscopy of picrosirius red stained sections, and anti-collagen I versus anti-collagen IV immunolabeling. We then identify the sources of noise that need to be corrected for in SHG images, and we propose suitable processing algorithms. We evaluate three fibrosis scores and show that they are appropriate for different types of collagen fibers distributions. Finally, using a morphological segmentation of the tissue based on endogenous 2PEF signals, we evidence preferred sites for fibrillar collagen accumulation in a murine model of renal fibrosis and show that SHG fibrosis scores are complementary to the usual scores related to non fibrillar collagen.

## 2. Advantages of SHG microscopy for visualizing and scoring fibrillar collagen

Ideally, a technique for imaging collagenous tissues should meet the following requirements: (i) High specificity for collagen, to enable quantitative scoring; (ii) Ability to distinguish between fibrillar and non fibrillar collagens; (iii) Three-dimensional (3D) visualization of the fiber's architecture; (iv) Simultaneous imaging of other tissue components, and versatility with respect to the tissue preparation method. Within this framework, we discuss in the following the specific advantages of SHG microscopy compared to conventional techniques.

### 2.1 Specificity of SHG microscopy for fibrillar collagen

We first verified the specificity of SHG signals. For that purpose, we compared SHG microscopy to immunohistochemistry, as the latter technique is highly specific and discriminates between various types of collagens. We studied serial thin sections of a fibrotic mouse kidney exposed to collagen I antibodies (AB765P, rabbit anti-mouse, Chemicon), collagen IV antibodies (AB756P, rabbit anti-mouse, Chemicon) or with no labeling. Secondary antibodies coupled with FITC (goat anti-rabbit, Chemicon) enable the visualization of the immunolabeling using fluorescence microscopy, and the 2PEF images are shown in Figs. 1(a) and 1(b). As expected, anti-collagen I immunolabeling underlines collagen I in the adventitia of the artery [Fig. 1(a)], and anti-collagen IV immunolabeling underlines collagen IV in the basal laminae in the media of the artery and around tubules [Fig. 1(b)]. We also recorded SHG images from these sections and compared the distribution of the SHG signal with the 2PEF signal from FITC. Figure 1(d) shows that SHG signals colocalize with anti-collagen I immunolabeling, in agreement with the literature [2, 4]. On the contrary, Fig. 1(e) shows that SHG does not colocalize with anti-collagen IV immunolabeling. This is confirmed using ImageJ colocalization algorithm (W. Rasband, National Institute of Health) whose results are displayed in white color in Fig. 1(g) and 1(h). 2PEF signals which do not

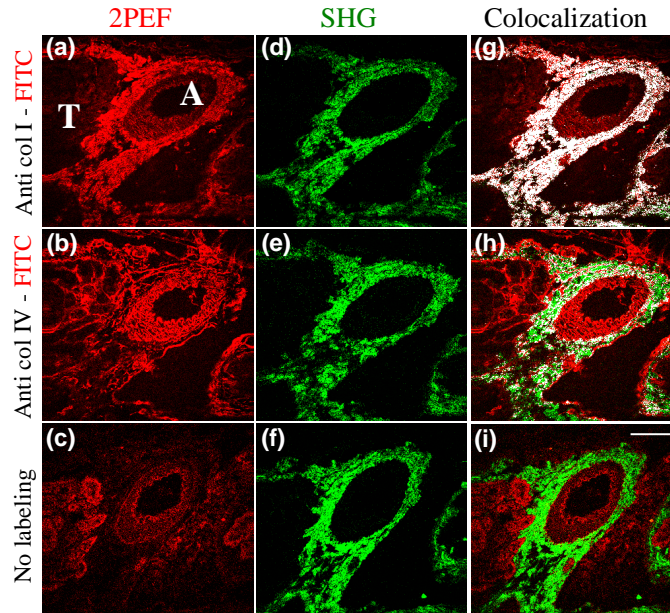


Fig. 1. Comparison of SHG imaging to immunolabeling of collagens type I and type IV in serial frozen sections of murine renal tissue showing artery (A) and tubules (T). (a-c) 2PEF signals from FITC-coupled antibodies revealing (a) collagen I or (b) collagen IV, and (c) from endogenous chromophores such as elastin or cellular chromophores. (d-f) SHG signals in the adventitia. (g-h) Colocalization (white) of 2PEF (red) and SHG (green) signals showing that SHG arises from collagen I, not from collagen IV. (i) Merging of (c) and (f) showing the distribution of endogenous signals. Excitation: 25 mW at 800 nm, 20 $\times$  0.9 NA objective, scale bar: 100  $\mu$ m.

colocalize with SHG signals in Fig. 1(g) correspond to endogenous 2PEF arising from elastic laminae in the media of the artery [10, 15, 16]. We verified that point by comparing Fig. 1(a) to Fig. 1(c) which displays the endogenous 2PEF image of an unlabeled section.

These results show unambiguously that collagen I generates second harmonic signals in tissues, and that collagen IV does not. We attribute these different behaviors to the different macromolecular organization of these two collagen types in tissues, because we previously reported that collagens I and IV present similar second-order nonlinear *molecular* responses (except for the chiral components) [11]: SHG signals in tissues are presumably dominated by coherent effects related to the high density and quasicrystalline order in collagen fibrils, and the absence of SHG signal from collagen IV in basement membranes results from the centrosymmetrical arrangement of this non fibrillar collagen.

## 2.2 Scoring of fibrillar collagen accumulation: SHG microscopy versus other techniques

The high specificity of SHG signals for fibrillar collagens results in an intrinsically small background in the images which enables sensitive measurements. In contrast, immunolabeling is considered as hardly quantitative despite its specificity, because this technique is highly sensitive to the accessibility of the epitope recognized by the antibody and to the yield of the *in situ* immunochemical reaction.

Collagen scoring is routinely performed using histological staining, as a cost-effective and simple technique. We therefore compared SHG signals and histological staining in a set of serial sections of fibrotic murine tissue. SHG images in Figs. 2(d) and 2(f) reveal that fibrillar collagen is located in the arterial adventitia and in the tubulo-interstitium. They also indicate that the glomerulus, which produces no signal, contains only non fibrillar collagen (type IV), as expected from immunochemical labeling (data not shown), and in agreement with the literature [17, 18]. In comparison, Fig. 2(a) shows that Masson's trichrome stains all

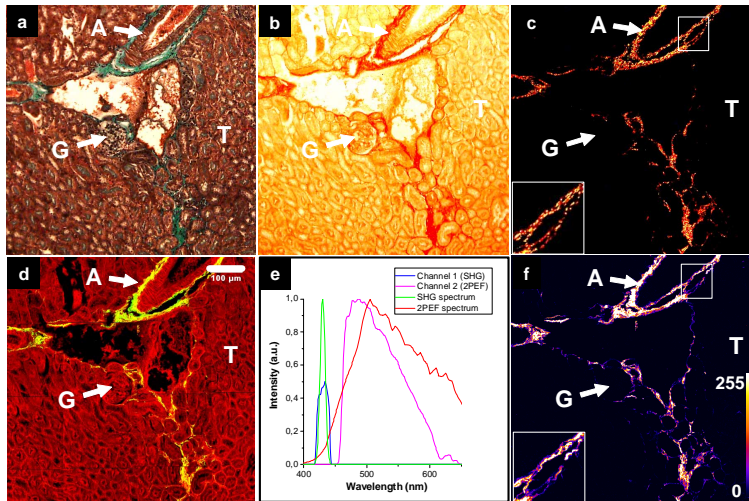


Fig. 2. Comparison of histological staining and endogenous SHG in fibrotic kidney tissue: serial sections of mouse kidney (4  $\mu\text{m}$  thick) visualized by (a-b) transmitted light microscopy, (c) polarized light microscopy, and (d,f) multiphoton microscopy (20 mW excitation at 860 nm, circular polarization, NA 0.9). G: glomerulus, A: artery, T: tubules, scale bar: 100  $\mu\text{m}$ . (a) Masson's trichrome staining; (b-c) Picrosirius red staining. (d) Multiphoton image showing SHG from collagen fibers (green) and endogenous 2PEF underlining the kidney morphology (red). (e) Spectra of these nonlinear endogenous signals (2PEF: red, and SHG: green), superimposed to the spectral transmittance of the SHG (blue) and 2PEF (pink) detection channels. (f) SHG image only (zoomed-in view in inset).

collagen types in green color, including collagen IV in the glomerulus, as well as other components of the extracellular matrix. Masson's trichrome therefore appears to be poorly specific, leading to confusion between fibrillar and non fibrillar collagen organizations. Consequently, it is difficult to obtain any accurate collagen scoring using this technique.

Picrosirius red staining is more specific for collagen, as exemplified in Fig. 2(b) where collagen appears in red. Moreover, it is then possible to specifically visualize fibrillar collagens using polarized light microscopy [19]. Comparison of standard transmitted light [Fig. 2(b)] and polarized light microscopy [(Fig. 2(c))] shows that non fibrillar collagen (type IV) in the glomerulus is slightly stained with Sirius red, but exhibits no contrast between crossed polarizers. On the contrary, collagen I around the artery is visible in both figures, because Sirius red staining enhances the birefringence of fibrillar collagen. The specificity of Sirius red staining for fibrillar collagen enables sensitive measurements, whose accuracy is related to the signal to noise ratio (SNR) in the image. This SNR is only limited by the accuracy of the extinction between the analyzer and the polarizer in the polarization microscope and by the natural heterogeneous birefringence of the tissue. It ranges typically from 10 to 100 depending on the area in the tissue, which is comparable to the SNR obtained with SHG microscopy.

We note that this technique is sensitive to the 3D orientation of the fibers, as exemplified in Fig. 2(c): only the fibers in the image plane and oriented at  $\pm 45^\circ$  from the polarizer (or analyzer) are correctly detected, and the image contains dotted structures, instead of continuous fibers (see inset). This artifact can be removed using circularly polarized light, which is however not routinely implemented in polarization microscopes, and slightly deteriorates the SNR in the image [20]. Finally, polarized light microscopy using picrosirius red staining is mainly limited by the variability in the staining protocols and in the induced birefringence, which limits the reproducibility of the measurements.

### 2.3 Versatility of SHG microscopy

The main advantage of SHG microscopy is its unique capability to provide 3D images of the organization of collagen fibers with micrometer resolution. Like other multiphoton

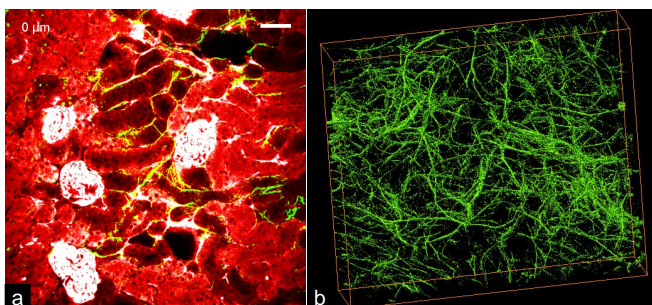


Fig. 3. (a). (1.3 MB) Multimodal multiphoton z-stack of a fixed fibrotic transgenic mouse kidney: the endogenous 2PEF signals (red) reveal the morphology of the tissue, the SHG signals (green) map the distribution of fibrosis and the 2PEF signals from eGFP (white) evidence the collagen synthesis sites (860 nm excitation, 6 mW for the eGFP and 28 mW for the endogenous signals, 50  $\mu\text{m}$  scale bar,  $488 \times 488 \times 44 \mu\text{m}^3$ , 13.4 s per image plane). (b) (2.3 MB) 3D reconstruction of SHG signal from collagen fibers in a fresh fibrotic mouse kidney (50 mW excitation at 860 nm,  $477 \times 406 \times 58 \mu\text{m}^3$ , 10.9 s per image plane).

microscopies, it indeed provides intrinsic optical sectioning, and is less sensitive to scattering in biological tissues than linear optical techniques such as confocal microscopy [21]. Moreover, this endogenous mode of contrast necessitates no staining, and is applicable to unlabeled sections. It enables the routine acquisition of z-stacks of 2D images from the surface of the tissue down to 50-100  $\mu\text{m}$  in depth, and the reconstruction of 3D images, as illustrated in Fig. 3. In comparison, histological and immunochemical techniques are only applicable to 2D thin sections. We note that SHG microscopy probes the second-order nonlinear tensorial response of the fibers in the focal volume, and is therefore sensitive to the orientation of the collagen fibers relatively to the laser polarization. In order to minimize these effects in the image plane, movies in Fig. 3 were acquired using circular polarization, like in polarized light microscopy.

Other attractive properties of this technique include its absence of bleaching and its versatility with respect to the tissue preparation: we have observed similar SHG signals from collagen fibers in fresh intact tissues, fixed tissues (with acetone, alcohol, PFA, or formalin) and frozen sections [14]. It is therefore possible to simultaneously record 2PEF signals from GFP/RFP constructs or any other chromophore requiring specific tissue preparations. It is also compatible with the visualization of lipid bodies using third harmonic generation microscopy [22]. In comparison, immunolabeling for collagen is restricted to cryosections, which can be preserved only for a few days unlike fixed sections. This procedure enables the simultaneous visualization of GFP constructs, but poorly preserves the cellular structures. As for picrosirius red staining, it requires alcoholic fixation of the tissue section, which is not compatible with the visualization of GFP constructs whose fluorescence is quenched in the presence of alcohol [23]. For instance, the section displayed in Fig. 2 was fixed with AFA (Alcohol-Formalin-Acetic Acid).

An example of the complementary nature of SHG and 2PEF microscopies is displayed in Fig. 2(d). Combined SHG/2PEF images permit the location of SHG signals from collagen fibers within the kidney, whose morphology is revealed by endogenous 2PEF signals. Both signals were acquired simultaneously in the backward direction by using a dichroic mirror (450DCLP, Omega) to separate 2PEF from SHG. Figure 2(e) shows the spectra of the multiphoton endogenous signals excited at 860 nm in the fixed renal tissue shown in Fig. 2(d), as recorded using a spectrometer (H10-61vis, Jobin-Yvon) on a descanned channel of the microscope. Collagen SHG at 430 nm is readily separated from endogenous 2PEF signal peaking around 510 nm, using appropriate filters to select the 2PEF signal (GG455 colored filters) or the SHG signal (interferential filter HQ430/20, Chroma). Spectral transmittances of these two detection channels are also depicted in Fig. 2(e). We note that the strong 2PEF signals we observed are characteristic for formalin fixed tissues and show similar spectra in the whole kidney.

To further illustrate the potential of combined SHG/2PEF microscopy, we also visualized eGFP constructs [24, 25]. We used a transgenic mouse where eGFP expression is controlled by the collagen I  $\alpha_1$  chain promoter [26]. It is then possible to compare the respective distributions of the sites of collagen I gene activation and the sites of collagen assembly into fibers in fibrotic mice, as depicted in Fig. 3(a). This movie shows a multimodal multiphoton z-stack combining endogenous 2PEF signal (red, kidney morphology), SHG signal (green, collagen fibers) and 2PEF signal from eGFP (white, collagen I gene activation) acquired upon 860 nm excitation. Multimodal microscopy combining SHG signals from collagen and 2PEF signals from GFP constructs should therefore prove particularly useful for deciphering the mechanisms of pathological accumulation of fibrillar collagen.

### 3. Accurate measurements of SHG signals from fibrillar collagen

#### 3.1 Multiphoton setup

Combined SHG/2PEF imaging was performed on a custom-built laser scanning microscope [10, 14, 22]. We used a 20 $\times$ , 0.95-NA objective lens (Olympus) in order to combine a large field of view and a good spatial resolution (typically 0.40  $\mu\text{m}$  (lateral)  $\times$  1.6  $\mu\text{m}$  (axial) near the sample surface). Multiphoton signals from thick tissue sections were excited in an upright geometry using epidetection. Second harmonic emission is usually stronger in the forward direction and depends on the organization of the harmonophores in the focal volume [27], but scattering may redirect a fraction of the forward-directed light towards the objective and contribute to some extent to the backward-detected signal in thick tissues. With 860 nm excitation, we conveniently detected backward SHG signals comparable in magnitude to intrinsic fluorescence signals in thick tissues. We adjusted the excitation power to typically 50 mW, and detected SHG signal from small fibers with negligible photobleaching of the 2PEF. We also inserted a quarter-wave plate on the laser path, resulting in a circular polarization just after the plate. Although this circular polarization was affected by the optical components in the microscope, sufficient excitation was maintained along any direction in the image plane to significantly improve the visualization of collagen fibers with any orientations in the image plane.

We always used the same acquisition conditions, so that no reference was needed to calibrate the measurements unless the pulse duration or focal volume changed due to small misalignments of the microscope or the laser cavity. For long-term experiments, we verified that there was no significant change in the SHG setup, using the dermis area of a formalin fixed skin biopsy as a reference.

#### 3.2 Corrections for the illumination variations

The laser intensity at focus is not perfectly constant across the field of view of the microscope and it decreases when penetrating within the sample because of scattering, absorption and optical aberrations. These variations in the illumination do not preclude accurate measurements, because they are the same for all samples. However, corrections are preferred for 3D reconstructions or when combining several images in order to map a large area in the tissue.

We corrected for vignetting in every 2D image using the 2PEF image from a fluorescent plastic slide acquired in the same conditions. We fitted the reference 2D image by a parabolic surface, and divided the raw SHG and 2PEF images by the normalized parabolic profile.

The contrast of sparse and thin collagen fibers decreases dramatically in a few tenths of microns when penetrating within biological tissues. Correction for the depth attenuation is therefore impeded by the SNR deterioration of the SHG signal and is not relevant for collagen scoring. For practical purposes, we only corrected our images for 3D visualizations, and we used the same correction as for endogenous 2PEF signals, considering that attenuation depths are mainly determined by the excitation attenuation and are comparable for 2PEF and SHG signals. We readily determined an average depth profile of the 2PEF signal in our samples, because these signals are uniformly distributed within the cortical tissue [see Fig. 3(a)]

compared to sparse SHG signals. We obtained an exponential attenuation as previously reported [28], and divided the SHG and 2PEF stacks by the normalized exponential profile. SHG data were usually undercorrected to preserve a reasonable SNR within the tissue, which amounted to underestimate the contributions from collagen fibers deep within the tissue.

### 3.3 Noise sources and corrections

The main source of noise in our SHG images is optical noise due to ambient stray light in the detector compartment and to fluorescence bleed through. The latter point is due to the blue edge of fluorescence passing through the interferential filter used on the SHG channel, as depicted in Fig. 2(e). This fluorescence background represents a small fraction  $K$  of the 2PEF images in a region with no collagen fibers. We also determined this ratio from the spectral transmittance of the SHG and 2PEF channels and the multiphoton spectra acquired on the descanned channel [see Fig. 2(e)]: we calculated the percentage of SHG and 2PEF signals on both channels, and obtained the  $K$  factor through matrix inversion. Both methods provided consistent results and we applied the correction schematized in Fig. 4 to the SHG images to remove the optical background:  $(SHG)_{corrected} = (SHG)_{raw} - C - (2PEF)_{raw} / K$ , where  $C=0.02$  reads for the ambient stray light (and for the dark counts in the detector, see below), and  $K=60$ .

The background in SHG images also arises from shot noise. We used photon counting photomultiplier tubes (Electron tubes, UK) with typically 20-100 dark counts per second. Shot noise scales as the square root of the number of detected photons, including fluorescence background. Although much smaller than the SHG signals from fibers, shot noise is present in the whole image whereas only small fibrotic areas exhibit significant SHG in our samples. It is therefore necessary to correct for this noise in order to improve the sensitivity of SHG measurements in heterogeneous fibrotic samples. For that purpose, we spatially filtered the SHG image using  $3 \times 3$  blurring and set a threshold as low as possible to obtain a mask. This procedure enhanced the contrast from extended structures containing low spatial frequencies such as fibers. We then applied this mask to the SHG image to remove the pixels with non significant SHG signal (see Fig. 4). The value of the threshold was kept constant for all images acquired in the same conditions, and for all depths within the tissue.

Figure 5 shows a corrected multiphoton image of a mouse fibrotic kidney, using the image processing summarized in Fig. 4. Sequential 2PEF and SHG z-stacks of  $270 \times 270 \times 40 \mu m^3$  were acquired simultaneously in the cortical region of a coronal section, with  $0.8 \times 0.8 \times 5 \mu m^3$  voxel size. We corrected the 2PEF images for vignetting and the SHG images for vignetting and noise, and we obtained large images of  $2300 \times 4600 \times 40 \mu m^3$ .

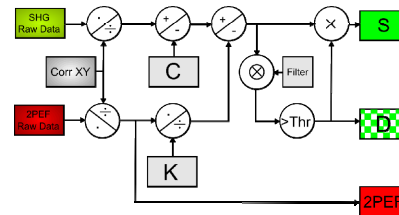


Fig. 4. Schematic of the image processing showing vignetting correction for 2PEF data, and vignetting correction, background correction and application of a threshold for SHG data. D stands for the mask image (pixel value=1 if significant SHG signal, 0 otherwise). S is the corrected SHG image where the pixels with no significant SHG signal are set to 0.

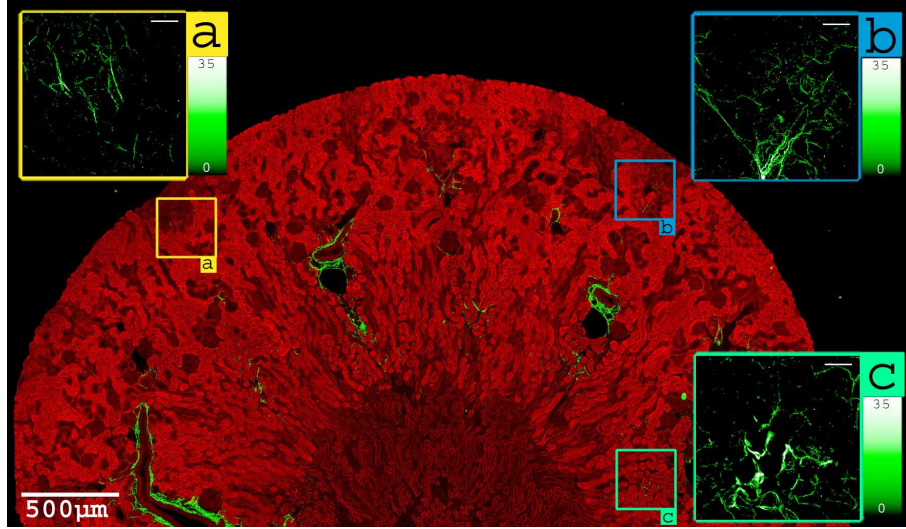


Fig. 5. (2.2 MB) Corrected 2PEF/SHG image mapping 2.3×4.6 mm<sup>2</sup> of an unlabeled fibrotic murine kidney with 0.8×0.8 μm<sup>2</sup> pixel size (2967×5865 pixels scanned at 100 kHz, with 20× 0.95-NA objective lens and 50 mW excitation at 860 nm, in a coronal fixed section). Intrinsic 2PEF signals (E700sp and GG455 filters, Chroma) arises from various cellular chromophores in the tubules and the collecting ducts, and SHG signals (E700sp and HQ430/20 filters, Chroma) map the distribution of fibrosis. The insets show the various distributions of collagen fibers scored in Table 1.

Table 1. SHG scoring of areas enlarged in Fig. 5.

Scores	Area (a)	Area (b)	Area (c)
D (density, %)	0.54	1.26	1.66
S (signal, arb. Units)	2.6	6.3	9.3
SF (signal in fibers)	4.8	5.0	5.6

### 3.4 Scoring

The detected SHG signal results from the coherent summation of the second harmonic fields radiated in the backward direction by all the collagen molecules within the focal volume ( $0.4 \times 0.4 \times 1.6 \mu\text{m}^3$  near the sample surface) [5, 27, 29-31]. However, collagen distribution is highly heterogeneous at this micrometer scale: the diameter of the collagen fibrils and fibers ranges from a few tenth of nm to a few μm, with variable molecular density and polarity within these structures [32]. Moreover, the collection efficiency of the SHG signal depends on the optical properties of the tissue, because scattering redirects a fraction of forward-emitted light towards the detector. Consequently, quantitative measurements of collagen by use of SHG microscopy are highly complex unless studying model systems with a well-known and homogenous distribution of collagen molecules. We therefore use a phenomenological approach to study biological tissues, and propose three different scores to probe the collagen distribution.

The first score is determined as the volume density of pixels exhibiting a significant SHG signal:  $D=[S_{\text{SHG}} > \text{threshold}]$ . It corresponds to the area of the mask used to remove the noise in a z-stack (D image in Fig. 4). The second score is determined as the average value of the SHG signal in the corrected SHG image (S image in Fig. 4):  $S = \langle S_{\text{SHG-corrected}} \rangle$ . The third score is determined as the average value of the corrected SHG signal in regions exhibiting significant SHG signals. It is obtained as the ratio of the two other scores:  $SF=S/D$ .

We calculated these scores in various regions of a fibrotic kidney exhibiting different collagen distributions. The corrected SHG images of these regions are displayed as insets in Fig. 5, and the scoring results are summarized on table 1. Inset (a) shows a few thin fibers, inset (b) shows a lot of thin fibers, and inset (c) shows larger fibers. Score D (density) readily discriminates between areas (a) and (b), i.e. between different quantities of small fibers. But it produces similar results for areas (b) and (c) where fibers exhibit different widths. Conversely, score SF (signal in fibers) discriminates between the latter distributions, because it takes the signal intensity into account, and fiber bundles produce higher SHG signal level than small fibrils. But it produces similar results for the two former distributions. These data show qualitatively that score D is sensitive to the extent of fibrosis in the tissue, whereas score SF probes the formation of larger and denser fibers or fiber bundles. Score S (signal) merges the two other scores and discriminates between all three areas, but it provides no information about the collagen organization. Overall, all these scores are informative, and their use depends on the particular distribution of fibrillar collagen in the tissue under study.

#### 4. Application to renal fibrosis

##### 4.1 Animal model

We studied a hypertensive model of renal fibrosis induced in C57Bl6 mice with chronic subcutaneous infusion of Angiotensin II and high salt diet. This model induces severe renal tubulo-interstitial fibrosis (accumulation of fibrillar collagen) along with sclerosis of the glomeruli (accumulation of non fibrillar type IV collagen), as attested by physiological and biochemical measurements (systolic blood pressure, albuminuria), and histological staining. In particular, renal damage is usually assessed using empirically defined glomerulosclerosis scores obtained as the percentage of pathological glomeruli observed on Masson's Trichrome histological sections [33]. These scores are relevant as far as they may be related to the renal filtration function, given that the glomeruli are the kidney filtering units. However, tubulo-interstitial fibrosis has proven to be a better predictor of progression of nephropathies to end-stage renal disease [34]. Its measurement by pathologists and investigators remains challenging, given that glomerulosclerosis scores, as well as systolic blood pressure and albuminuria measurements or hydroxyproline assays (measurement of the collagen content of the tissue) do not specifically probe fibrillar collagens.

We therefore compared control and fibrotic mice using SHG microscopy. Mice were euthanized after 49 days and kidney were removed and fixed in PBS buffered 4 % formaldehyde. 200  $\mu\text{m}$  thick coronal sections were cut at a reproducible position within the kidney (1/4th of the height from the superior part of the kidney) and they were scanned using the protocol detailed in the former section.

##### 4.2 Fibrosis distribution in various regions of interest

Combined 2PEF/SHG images in Fig. 5 clearly evidence a tubulo-interstitial fibrosis in treated mice, as already noted in Fig. 2(d). The distribution of collagen fibers around the tubules and the arterioles is better revealed in z-stack movies and 3D reconstructions, as exemplified in Fig. 3 and associated movies. We note that the fibrosis distribution is highly heterogeneous, which implies that large regions must be mapped in the kidney to obtain relevant SHG data. In practice, we scanned  $2.5 \times 5 \text{ mm}^2$  areas in all our samples, with  $0.8 \times 0.8 \mu\text{m}^2$  pixel size, which allowed us to detect small collagen fibers heterogeneously dispersed in the whole tissue. We usually acquired 8 images every 5  $\mu\text{m}$  within the tissue, and obtained finally 500 MB of data after typically 90 minutes of acquisition with 100 kHz pixel rate and 15 minutes of data processing. The actual resolution of the multiphoton image is better seen when zooming in Fig. 5 (see supplementary materials).

Analysis of the SHG image in Fig. 5 reveals variable collagen organizations depending on renal regions. It is better seen in Fig. 6 where the 2PEF [Fig. 6(a)] and SHG [Fig. 6(b)] images are shown separately. The superficial cortex contains small fibers, whereas larger fibers accumulate in the deep cortex near arteries. We therefore defined regions of interest using a

radial segmentation of the coronal section to take into account the radial symmetry of the kidney morphology. Segmentation was adjusted to the particular morphology of every

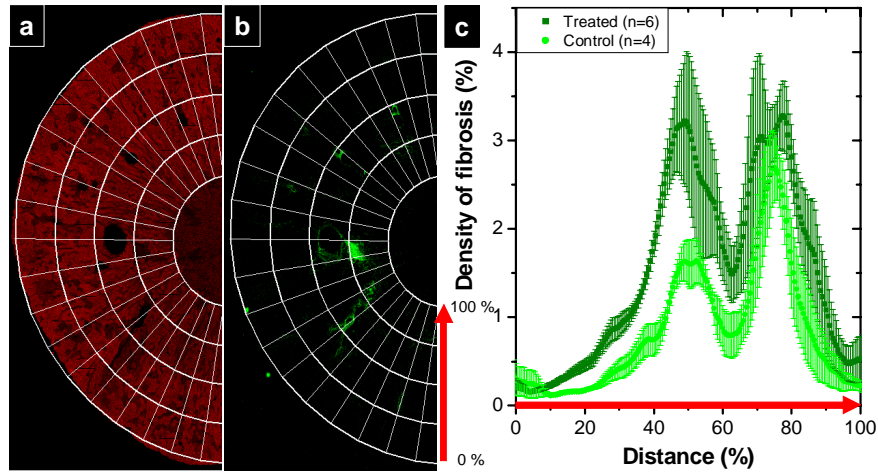


Fig. 6. Morphological segmentation and SHG fibrosis scoring in the renal cortex of control versus treated mice. (a) Endogenous 2PEF image revealing the renal morphology and (b) SHG image evidencing collagen fibers, superimposed with the radial segmentation from the capsule (0%) to the papilla (100%) in the same unlabeled fibrotic kidney tissue as in Fig. 5(c). D score, expressed as a volume density of fibrosis, along the kidney cortex in control (light green) and Angiotensin II infused mice (dark green). Error bars correspond to standard errors of the mean.

Table 2. SHG scoring of control versus treated mice. Error bars correspond to standard errors of the mean.

Scores	Control	Treated
D (density, %)	$0.74 \pm 0.09$	$1.37 \pm 0.11$
S (signal, arb. units)	$6.6 \pm 1.0$	$13.9 \pm 1.5$
SF (signal in fibers)	$8.9 \pm 0.6$	$10.1 \pm 0.6$
Sclerosed glomeruli (%)	$8 \pm 2$	$79 \pm 2$

kidney sample taking advantage of the 2PEF image which underlines its main morphological features, and fitting the renal capsule and the renal papilla using conical curves (see 0% and 100% curves in Fig. 6). We then scored all the ring-shaped regions to assess the fibrosis as a function of the distance to the renal capsule.

#### 4.3 Results and discussion

We calculated the three SHG scores proposed in section 3, and Fig. 6(c) presents the results obtained from 4 control mice and 6 treated mice using score D. This score appeared to be the most appropriate to account for the specific distribution of collagen fibers during renal fibrosis. It is particularly sensitive to the small fibers developing in the superficial cortex, which seem to be highly characteristic of fibrotic mice as attested by the small error bars.

Most importantly, all these scores sort out control and fibrotic mice with only a few samples, as shown on table 2 which presents averages of the 3 scores on the whole cortex. The statistics may be further improved by studying more animals; however, they unambiguously show that SHG microscopy is a reliable method to assess renal fibrosis.

Finally, we compared these results to conventional scores of glomerulosclerosis determined on histological thin sections obtained from the other kidney of the sacrificed animals [33]: table 2 displays the percentage of pathological glomeruli, which increases dramatically for the treated mice compared to the control ones. We note that SHG scoring is

in qualitative agreement with this conventional score. Quantitative discrepancies may be attributed to the difference in the collagen types and in the renal compartments probed by the 2 methods: glomerulosclerosis results from the accumulation of collagen IV and other matrix components in the glomerulus, whereas SHG probes fibrillar collagens in the renal interstitium. Our results show that the main affection of mice infused with Angiotensin II for 49 days corresponds to sclerosis of the glomeruli, whereas a few fibers appear in the interstitium. However, regression of glomerulosclerosis has already been observed, whereas interstitial fibrosis has been shown to evolve to severe nephropathies [34]. Detection of moderate fibrosis is therefore of great interest for physiopathologists, as already noted before, and SHG microscopy appears as a sensitive method for that purpose. The two methods then give complementary information and their detailed correlation in a multimodal approach should improve the assessment of fibrosis progression or regression.

## 7. Conclusion and perspectives

In this study, we showed that SHG microscopy presents unique advantages compared to conventional optical techniques to investigate the 3D heterogeneous accumulation of fibrillar collagen during fibrotic pathologies. Importantly, we unambiguously proved that SHG is obtained specifically from fibrillar collagen in tissues, by comparing anti-collagen I versus anti-collagen IV immunohistochemical labeling. This specificity results in an intrinsically small background noise in the images, due mainly to fluorescence bleed through and shot noise, and readily corrected for using appropriate image processing. The high signal over noise ratio in the corrected images then enables sensitive measurements of the fibers extent in the tissue. Furthermore, the ability of SHG microscopy to discriminate between fibrillar and non fibrillar collagen is of invaluable interest to study fibrotic pathologies. As previously noted, measurements of the accumulation of fibrillar collagens provide better scores of severity for pathologists than scores related to non fibrillar collagen.

We therefore proposed phenomenological scores based on the volume density of voxels exhibiting significant SHG signal and on the SHG averaged intensity. We demonstrated that the SHG density score is sensitive to the accumulation of small collagen fibers, whereas the SHG intensity score probes the formation of larger fibers. We used endogenous 2PEF signals in a multimodal approach to visualize the tissue morphology and perform relevant image segmentation. We then measured the SHG density and intensity scores in a murine model of hypertensive renal fibrosis, and successfully sorted out control and treated mice. We also evidenced accumulation of fibrillar collagen in the renal interstitium, which proved that other renal compartments than the glomerulus are affected during hypertensive nephropathies. The scores we proposed here should therefore help to elucidate the role of various enzymes related to the collagen assembly into fibers and to test possible inhibitors.

We anticipate that this protocol will be adjustable to other organs such as the liver and the cardiovascular system. In combination with 2PEF imaging of collagen synthesis sites using GFP constructs in transgenic animal models, SHG microscopy should prove a valuable tool to investigate extracellular matrix remodeling in various pathologies.

## Acknowledgments

The authors thank J.M. Sintès and X. Solinas for expert technical assistance. M. Strupler was supported by a grant from Région Ile de France. A.-M. Pena was supported by a grant from “Fondation pour la Recherche Médicale”.